Title: Phosphorus stress and spatial confinement lower the threshold for quorum-sensing activation of redox-active metabolite production in *Pseudomonas synxantha*

Authors: R. E. Alcalde[1], H. Jeckel[1], O. Zhang[2], R. L. Avila[1], N. Dalleska[3], D. Mavrodi[4], C. Yang[5], D. K. Newman[1,6,a]

[1]Division of Biology and Biological Engineering, California Institute of Technology, Pasadena, CA 91125

[2]Department of Physics & Astronomy, Texas A&M University, College Station, TX 77843

[3]Global Environmental Center, California Institute of Technology, Pasadena, CA 91125

[4]USDA, Agricultural Research Service, Wheat Health, Genetics and Quality Research Unit, Pullman, Washington, USA

[5]Division of Engineering and Applied Science, California Institute of Technology, Pasadena, CA 91125

[6]Division of Geological and Planetary Sciences, California Institute of Technology, Pasadena, CA 91125

[a]To whom correspondence may be addressed. Email: dkn@caltech.edu

Abstract:

Bacteria often coordinate collective behaviors such as biofilm formation and secondary metabolite production through quorum sensing (QS), a regulatory system traditionally linked to high cell density. However, in environments like soil, where microbial populations are spatially fragmented, sparse, nutrient-limited, and subject to mass transport, the mechanisms that enable QS-dependent processes remain incompletely understood. Here, we investigate the regulation of a secreted redox-active metabolite, phenazine-1-carboxylic acid (PCA), in *Pseudomonas synxantha* 2-79, a model rhizobacterium, under phosphorus (P) limitation, a persistent stress in many soils. Using a combination of microscopy and molecular genetic approaches, we show that P limitation sensitizes the QS activation threshold by an order of magnitude, enabling phenazine induction at relatively low population densities in

comparison to P replete conditions. This induction is abolished in QS-deficient mutants and restored by the addition of exogenous acyl-homoserine lactone (AHL), demonstrating that quorum sensing remains essential but its threshold becomes environmentally tuned. Under P limitation, spatial confinement and pore saturation levels further shape the timing and location of induction, illustrating how physical structure and nutrient stress can modulate bacterial activities. Moreover, phosphorus stress confers both collaborative and competitive advantages, enabling *P. synxantha* to undergo low-cell density AHL cross-talk between related *Pseudomonas* spp. and to suppress other rhizobacteria. Lastly, on plant roots, PCA genes are more predominantly induced under P limitation. These findings illustrate how the nutrient status of an environment can modulate the onset of quorum sensing, enabling quorum-regulated behaviors to activate at lower thresholds.

Introduction:

Soil microbes sustain ecosystems. Through their metabolism, they drive nutrient cycling, modulate plant health, and influence mineral weathering. Many of these functions depend not only on individual physiology but on the coordinated activity of microbial populations and communities, often mediated through the release of small molecules that act as public goods, chemical signals, or antibiotics. Among these, phenazines—redox-active metabolites produced by diverse soil bacteria that support a variety of biological functions[1–4]—are particularly notable. Through their redox chemistry, they promote phosphorus[5,6] and iron availability,[7–10] shape microbial competition,[11–13] and affect plant-microbe interactions[14–16] in the rhizosphere.

Phenazine biosynthesis is typically controlled by quorum sensing (QS), a gene regulatory system in which bacteria produce and respond to diffusible signals, such as acyl-homoserine lactones (AHLs), to coordinate group-level behaviors.[17,18] Once a threshold concentration of signal accumulates, often reflected by high cell density, QS activates gene expression for costly cooperative functions like biofilm formation, virulence, or secondary metabolite production.[19–25] This framework is well supported in

48 laboratory systems. However, in natural environments like soil, microbial populations are often spatially
49 fragmented, sparse, and physically confined within pore structures,[26–28] conditions that can shift signal
50 accumulation and QS activation. Cluster analyses in structured soils report that larger clusters (>100 cells)
51 become sparse as water content decreases, implying many neighborhoods fall below 100 cells.[26] Despite
52 this, phenazines[29,30,4], and other QS-regulated metabolites[31–33] are commonly detected in the rhizosphere.
53 How, then, are these behaviors triggered in environments where signal accumulation may be restricted?

54 Several models emphasize that QS dynamics also depend on environmental structure and signal transport.
55 Diffusion sensing and efficiency sensing, alternative descriptions of quorum sensing, describe how mass
56 transfer, spatial confinement, and local cell organization determine whether signal concentrations reach
57 activation thresholds.[34–37] In structured habitats like biofilms and soils, spatial confinement and mass
58 transfer limitation may allow signals to accumulate locally even when bulk population density is low.[28,38–
59 41] Consistent with this view, a few single cells confined in picoliter microfluidic chambers initiate "high-
60 density" QS programs.[38] Likewise, flow cell experiments show that advection suppresses QS in exposed
61 regions of a biofilm while sheltered niches maintain activation.[42]

62 Beyond physical structure and transport, rhizosphere chemistry and biology, such as nutrient limitation,
63 physicochemical stress, and host-derived cues can also tune QS induction[43]. Here we focus on
64 phosphorus limitation in *Pseudomonas synxantha* (formerly *P. fluorescens*) 2-79, a plant growth-
65 promoting rhizobacterium that produces phenazine-1-carboxylic acid (PCA).[44,45] In this strain, PCA
66 production is governed by a single AHL-based quorum-sensing system, PhzIR; deletion of either *phzI* or
67 *phzR* abolishes PCA production.[45–47] Although PCA increases under phosphorus limitation,[6,48] whether
68 this induction is mediated by the PhzIR circuit, arises via cross-talk with other QS pathways, or is driven
69 independently of QS remains unknown. This organism-level question is motivated by the broader soil
70 context: freely available inorganic phosphate is extremely low because much of it is immobilized through
71 sorption to mineral surfaces, [49–51] and in *Pseudomonas aeruginosa*, phosphate (and iron) limitation is

72 known to influence secondary metabolism through multiple QS pathways (e.g., PQS, IQS, RhlR)[52–58] via
73 the PhoBR two component that governs system central phosphate sensing and response.[59–61]

74 We set out to determine whether phosphorus stress alters QS dynamics in *P. synxantha* 2-79. Specifically,
75 we asked whether phosphorus-limited induction of PCA is QS-dependent or QS-independent. We
76 postulated that phosphorus stress would trigger AHL-based PhzIR circuits, thereby lowering the effective
77 QS cell density threshold because PCA production under P limitation occurs at lower cell densities in
78 comparison to standard conditions.[48] We further hypothesized that structured environments act with
79 phosphorus levels to shape the onset, location, and ecological consequences of QS-regulated behaviors.
80 To test these predictions, we integrated genetic, optical, and ecological approaches to better understand
81 the rules governing microbial coordination in nature.

82 **Results**

83 **Phosphorus limited environments enhance phenazine gene expression of *Pseudomonas synxantha* in**
84 **plant root microcosms**

85 To begin exploring how phenazine biosynthesis responds to phosphorus availability in the rhizosphere,
86 we imaged *Pseudomonas synxantha* 2-79 colonizing *Brachypodium distachyon* Bd21-3 roots under
87 phosphorus-replete (P-rep; excess inorganic phosphate in medium), phosphorus-limited (P-lim; no
88 inorganic phosphate in medium), and phosphate-sequestering (P-HFO; phosphate bound to iron, i.e., not
89 bioavailable) conditions using light sheet fluorescence microscopy (LSFM). In many Fe-oxide–rich,
90 acidic to neutral soils, phosphate is strongly retained by iron oxides (e.g., hydrous ferric oxide,
91 HFO),[50,62,63] so our P–HFO treatment approximated this sequestration. A dual fluorescent reporter was
92 used to track phenazine biosynthesis gene expression (P_{phzA}-GFP, green channel) and colonization density
93 readout (constitutive, P_{tac}-mCherry, red channel). Fluorescence intensity was quantified from maximum
94 intensity projections (MIPs) of LSFM images. For each object within a region of interest, the mean

95 intensity was calculated as integrated density divided by object area. This metric approximates
96 fluorescence per unit area in 2D projections, serving as a readout for relative reporter expression and cell
97 density in colonized regions. Bar plots and Empirical Cumulative Distribution Functions (ECDFs)
98 revealed condition-specific differences in both fluorescence magnitude and distribution (Fig. 1A–B).

99 Induction of phenazine biosynthesis (P_{phzA}) was highest under the P-HFO condition (mean = 0.138),
100 followed by P-lim (mean = 0.061), while remaining minimal under P-replete conditions (mean = 0.016).
101 Although the P-lim condition exhibited lower average expression than P-HFO, its distribution was
102 markedly right-skewed and heavy-tailed, indicating rare but strong induction events. In contrast, P-HFO
103 displayed a broader, moderate distribution, while P-rep remained narrowly distributed around low
104 fluorescence values (Fig. 1B). Representative LSFM images corroborated these findings, revealing robust
105 activation of the P_{phzA} reporter under P-HFO but not under P-replete conditions (Fig. 1C). Interestingly,
106 phenazine expression did not directly correlate with cell density. The constitutive reporter was highest in
107 P-HFO and P-rep (means = 0.117 and 0.115, respectively) and lower under P-lim (mean = 0.051), yet
108 only P-lim and P-HFO conditions induced the phenazine reporter.

109 These observations indicate that at the time of measurement, the cell density was insufficient to trigger
110 phenazine gene expression under nutrient-replete conditions. How, then, does phosphorus limitation
111 stimulate phenazine gene induction at local colonization levels that fail to trigger expression under
112 phosphorus-replete conditions? This observation suggests that canonical QS induction of phenazines may
113 be altered under nutrient stress, but whether this results from a bypass of QS regulation, an increased
114 sensitivity to quorum signals, or integration with parallel stress-response pathways was unclear. We set
115 out to disentangle these possibilities.

116

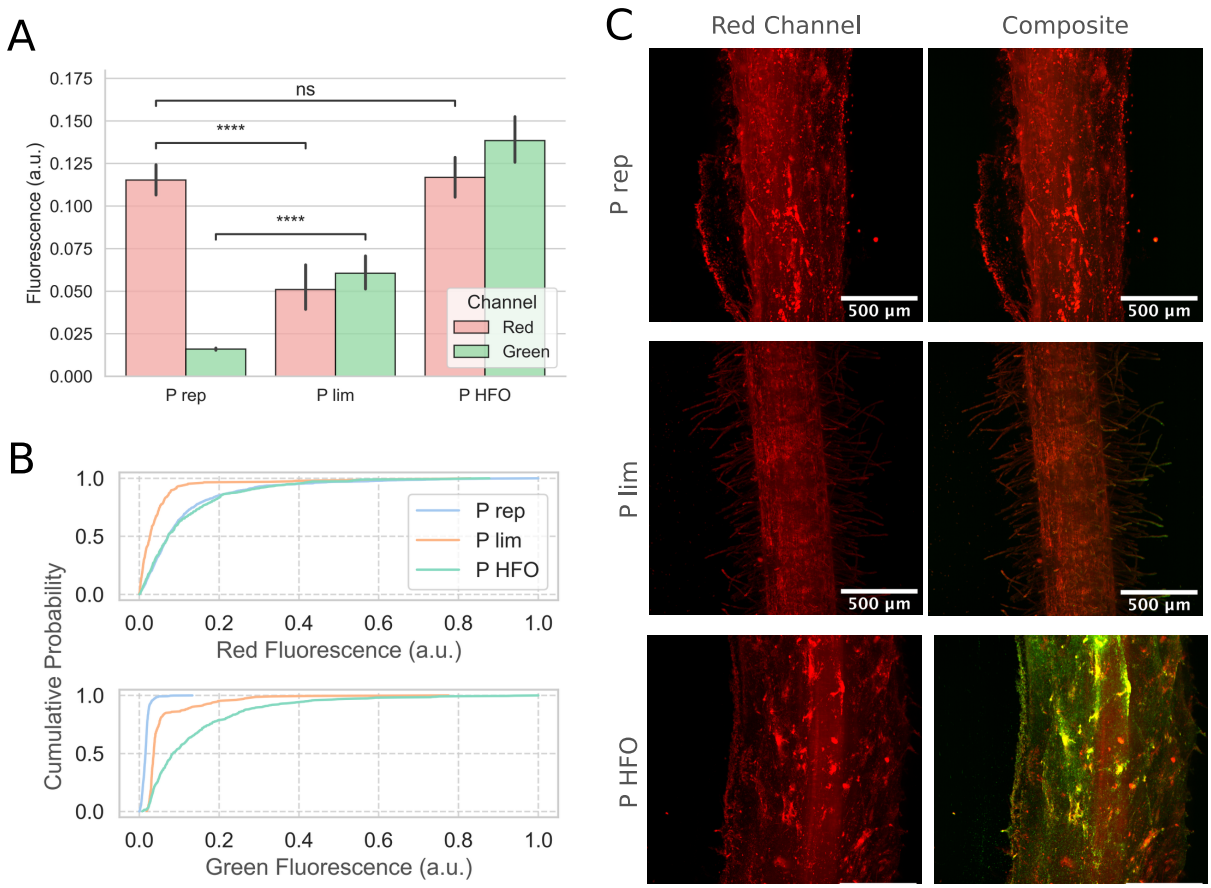

Figure 1: Phenazine gene expression of *Pseudomonas synxantha* 2-79 on plant roots under different phosphorus conditions. (A) Bar plots showing mean ± 95% CI of normalized red channel (constitutive; P_{tac}) and green channel (phenazine biosynthesis; P_{phzA}) fluorescence intensities under phosphorus-replete (P-rep), phosphorus-limited (P-lim), and phosphate-sorbing hydrous ferric oxide (P-HFO) conditions. Statistical comparisons were performed using two-sided Mann–Whitney tests; significance is indicated by asterisks (ns, not significant; **** $p < 0.0001$). **(B)** Empirical cumulative distribution functions (ECDFs) of normalized fluorescence intensities from the same dataset shown in (A), illustrating the distribution of object-level fluorescence values across experimental conditions. **(C)** Representative maximum intensity projection (MIP) images acquired by light sheet fluorescence microscopy (LSFM) of *P. synxantha* colonizing plant roots under P-rep, P-lim and P-HFO conditions. Red channel images (left) are shown with identical intensity thresholds to compare red fluorescence. Composite images (right) overlay red and green channels using the same fixed thresholds across conditions, revealing differences in P_{phzA} reporter induction. Scale bars = 500 µm. See also Movie S1 for a 3D reconstruction, Table S1 for summary statistics, and Figure S1 for object-level strip plot.

Quorum sensing is required for phenazine production under phosphorus limitation, and phosphorus stress sensitizes the QS system to AHL.

134 To determine whether phenazine production under phosphorus limitation requires the *phzIR* quorum
135 sensing (QS) pathway, we examined wild type and mutants defective in either the phenazine production
136 genes (*phzA*-*G*), the QS signal synthase (*phzI*), or the phosphorus starvation response regulator (*phoB*)
137 under P-rep (7 mM Pi) or P-lim (100 μM Pi) conditions in 96-well plate liquid cultures (Fig. 2A). The
138 wild type produced phenazines under both conditions but showed markedly higher induction per cell
139 under P-lim. In contrast, the Δ*phzI* mutant failed to produce phenazines under P-lim and P-rep,
140 confirming that QS is required for induction under P-lim. Similarly, the Δ*phoB* mutant did not produce
141 phenazines under P-lim but retained production under P-rep, indicating that phosphorus stress signaling
142 via PhoBR is also required in the P-lim response.

143 We next asked whether exogenous addition of the QS signal produced by PhzI would complement Δ*phzI*
144 and whether this response is specific to phosphorus depletion. We performed a dose–response assay by
145 supplementing the Δ*phzI* mutant with the N-(3-hydroxy-hexanoyl)-L-homoserine lactone (3-OH-C6-
146 HSL) (Fig. 2B). *P. synxantha* produces at least six AHLs, including three of the hydroxy form, with 3-
147 OH-C6-HSL having the highest sensitivity to the PhzR.[46] To restrict growth and isolate regulatory
148 effects, we used a defined buffer medium lacking either nitrogen (No-N) or both nitrogen and phosphorus
149 (No-N/P). After 20 h, PCA production was absent in No-N cultures, even at high QS signal
150 concentrations, but was strongly induced in No-N/P cultures in a dose-dependent manner.

151 We further asked whether phosphorus limitation increases sensitivity to QS molecules. We therefore
152 performed a second 3-OH-C6-HSL dose–response assay (Fig. 2C), this time allowing the Δ*phzI* mutant to
153 grow under P-rep (7 mM) and P-lim (100 μM) conditions. After 20 h, PCA production was present in
154 both conditions in a dose-dependent manner, but under P-lim, lower QS signal concentrations were
155 sufficient to induce phenazine production. Fitting a two-parameter Hill (log-logistic) function revealed
156 half-maximal effective concentrations (EC50) of 0.51 μM (P-rep) and 0.05 μM (P-lim), indicating ~10-
157 fold greater sensitivity under phosphorus stress.

158 Lastly, to verify QS signal production, we directly quantified AHLs (i.e., 3OH-C6-HSL, 3OH-C8-HSL,
159 and 3OH-C10-HSL) by LC-MS under P-rep, P-lim, and N-lim (nitrogen limited) conditions for both the
160 wild-type strain and Δ*phzI*. Results are shown for WT (Fig. 2D). For the wild-type strain, QS signals were
161 produced under both P-lim and P-rep but were not detected under N-lim. No AHLs were detected with the
162 Δ*phzI* strain. 3OH-C10-HSL was not detected under any conditions. Our limit of detection was 10 nM for
163 all AHLs.

164 Together, these results demonstrate that phenazine production under P-lim is QS-dependent and requires
165 the PhoBR two-component system. Moreover, phosphorus stress sensitizes QS by lowering the AHL
166 activation threshold, enabling induction at levels that are non-inducing under P-rep or N-lim.

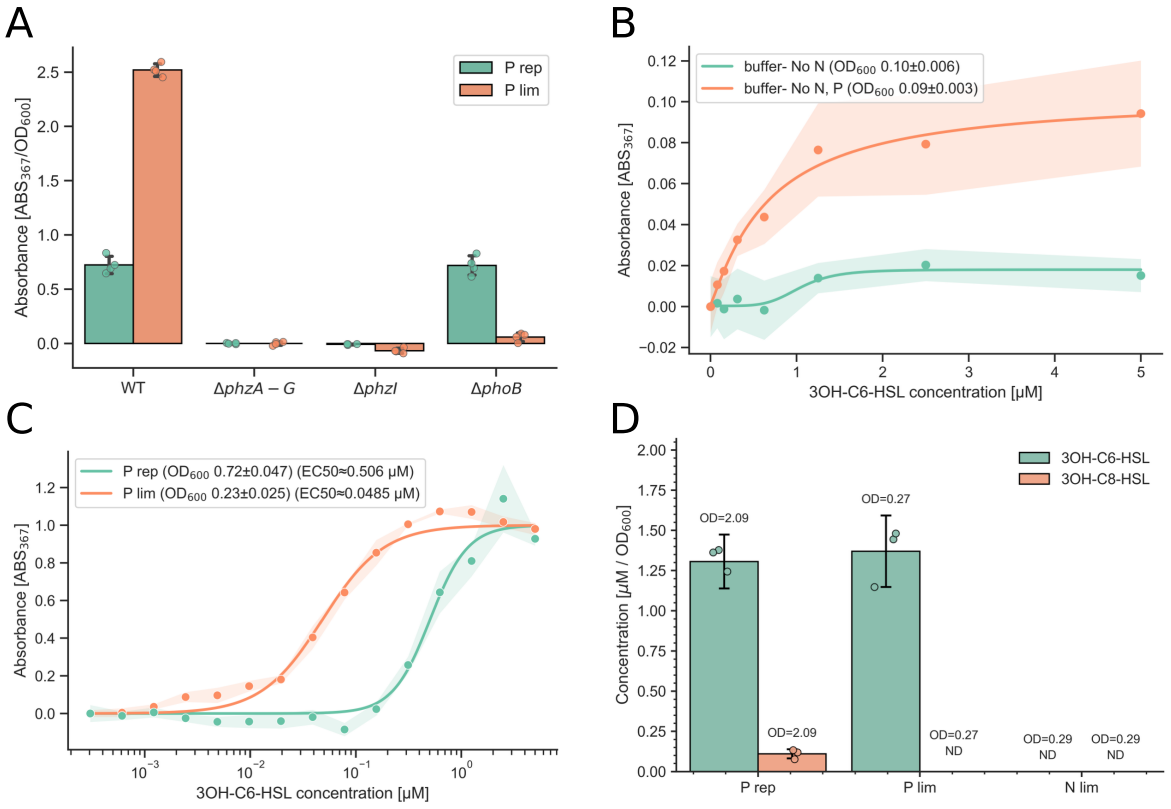

167

168 **Figure 2: Quorum sensing requirement and reduced AHL concentration threshold for phenazine**
169 **production in *Pseudomonas synxantha* 2-79 under phosphorus limitation. (A)** Phenazine-associated
170 absorbance normalized to cell density ($ABS_{367} \cdot OD_{600}^{-1}$) in *P. synxantha* strains under phosphorus-replete
171 (P-rep) and phosphorus-limited (P-lim) medium at 20 h post-inoculation. Values were baseline-corrected

using the Δ*phzA-G* mutant mean for each condition. Bars show mean ± SD of replicates; points represent individual measurements; n=4. **(B)** Dose–response of the Δ*phzI* mutant strain to exogenous 3-OH-C6-HSL under nitrogen-free (No-N) and combined nitrogen- and phosphorus-free (No-N, P) conditions at 20 h post-inoculation. Responses were baseline-corrected by subtracting the mean signal at 0 μM 3-OH-C6-HSL within each condition. Points show per-dose means; shaded regions indicate mean ± SD of replicates; n=5. Curves show four-parameter logistic model fits. Insert in legend: mean ± SD of OD_{600} at the assay timepoint. **(C)** Dose–response of the Δ*phzI* mutant strain to exogenous 3-OH-C6-HSL at 20 h under P-rep and P-lim medium at 20 h post-inoculation. Responses were baseline-corrected and scaled to an empirical E_{max} (median of the two highest doses) to yield 0–1 normalization. Points show per-dose means; shaded bands indicate ±SD across replicates; n=3. Curves are two-parameter Hill fits; Insert in legend: mean ± SD of OD_{600} at the assay timepoint and EC_{50} values from the fits. **(D)** AHL concentration normalized to cell density (μM · OD_{600}^{-1})) for 3OH-C6-HSL and 3OH-C8-HSL across P-rep, P-lim, and nitrogen-limited (N-lim) conditions. Bar plots show mean ± SD. Values above each bar indicate the corresponding optical density (OD_{600}) at sampling time (22 h). "ND" denotes values below the detection limit.

Phosphorus limitation enables quorum sensing activation at low cell densities in planktonic culture

Because QS is required for phenazine production under P-lim, we inferred that phosphorus stress decreases the cell-density threshold for QS activation. To test this, we used reporter strains to track QS-dependent induction in wild type *P. synxantha* 2-79 grown in well-mixed liquid culture across phosphate regimes (25, 100, and 7000 μM Pi) with or without exogenous 3-OH-C6-HSL (AHL) (Fig. 3A-B). Our previously constructed P_{phoA} and P_{phzA} reporter strains[48] served to monitor phosphorus stress (activation of PhoBR) and phenazine production, respectively.

The *phoA* reporter was induced in mid-exponential phase at 25 and 100 μM Pi (P-lim), with both induction timing and cell density increasing with phosphorus availability. It was not detected at 7000 μM Pi (P-rep). Without added AHL, the *phzA* reporter was induced in late exponential/early stationary phase under all conditions, but earlier and at a substantially lower cell density in P-lim compared to P-rep (OD_{600} at induction: 25 μM, 0.0846 ± 0.001; 100 μM, 0.219 ± 0.005; 7000 μM, 0.806 ± 0.006; mean ± SD), representing ~10-fold and ~4-fold reductions at 25 and 100 μM, respectively. Addition of exogenous AHL advanced induction time and lowered the density threshold further; under P-lim. Moreover, *phzA* onset aligned more closely with *phoA*, consistent with phosphorus stress priming the QS response while endogenous signal accumulation is rate-limiting when AHL is not supplied. It is also noteworthy that

203 even when AHL is exogenously added in excess, gene expression still requires the cells to be under P
204 limitation or relatively high cell density under P-rep for induction. That is, it seems that beyond requiring
205 high AHL concentrations the cells need to be in a state of physiologically readiness (e.g., P stress, other
206 stress responses at high cell density).

207 These results indicate that phosphorus stress reduces the cell-density requirement for quorum activation
208 and speeds QS-dependent gene expression in well-mixed cultures, motivating tests in structured
209 environments that better simulate rhizosphere matrices, where mass transfer and bacterial confinement
210 could further tune this sensitization.

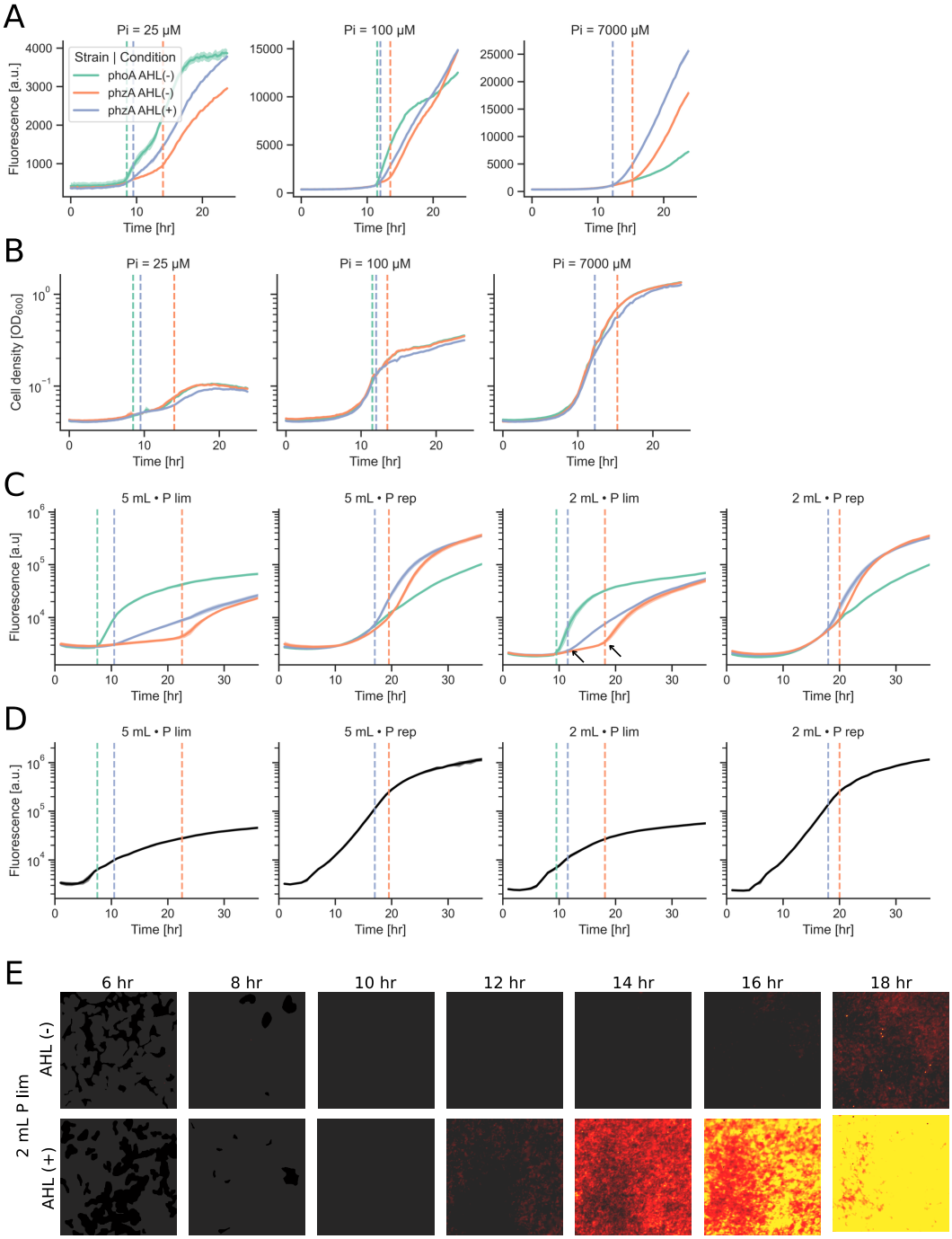

Figure 3: Induction benchmarks and growth dynamics under phosphorus regimes of planktonic and sessile *Pseudomonas synxantha* 2-79 cultures. (A) Induction curves for phosphorus-stress (*phoA*) and phenazine biosynthesis (*phzA*) reporters in liquid cultures across phosphate regimes (Pi = 25, 100, 7000 μM). Raw fluorescence intensity values are shown. **(B)** Growth curves in liquid cultures as cell density (OD_{600}). **(C)** Induction curves for *phoA* and *phzA* in agar biofilms under P-lim and P-rep conditions in either 5 mL or 2 mL agar volumes. Raw fluorescence intensity values are shown. **(D)** Growth curves in agar biofilms represented by the constitutive reporter fluorescence intensity (cell

219 density readout). **(E)** Representative images of reporter induction time course for biofilms grown under P-
220 lim in a 2 mL agar volume. Intensity of fluorescence is depicted by red to yellow hue. Gray shading
221 denotes the area coverage of aggregates. Legend: WT P_{phoA} without AHL addition (green), WT P_{phzA}
222 without AHL addition (orange), P_{phzA} with AHL addition (blue). Curves denote mean; shading denotes ±
223 SD; n = 3. Error not seen is smaller than the line. Dashed vertical lines mark reporter induction times.
224 Arrows on third graph correspond to images in (E)

225

226 **Phosphorus limitation also lowers the cell density threshold for quorum sensing activation in sessile**
227 **populations**

228 We employed an early-stage colony–biofilm assay using our previously developed imaging system[48] to
229 quantify growth and reporter expression in *P. synxantha*. In this diffusion-dominated context, AHL
230 concentrations in the biofilm arise from the balance between signal production, diffusive loss into the
231 underlying agar (which serves as a sink), and retention within the biofilm matrix. Reporters on
232 phosphorus stress (P_{phoA}) and phenazine production (P_{phzA}) tracked induction, and a constitutive reporter
233 ($P_{PA10403}$) provided a readout for cell density (Fig. 3C-E). By varying nutrient status, agar volume, and
234 AHL supplementation, we modulated regulatory sensitivity, sink capacity (5 mL vs 2 mL agar volumes),
235 and signal availability, respectively, to reveal how these factors shape QS activation.

236 5 mL agar: Under P-lim, *phoA* was detected early (~7.5 hr), but *phzA* induction was markedly delayed
237 (~22.5 hr). Under P-rep, *phoA* did not induce (as expected), whereas *phzA* induced at 19.5 h. This pattern
238 is opposite to planktonic cultures, where P-lim induces earlier than P-rep, indicating that in this
239 heterogeneous, diffusion-dominated context, QS-signal accumulation is delayed under P-lim.
240 Notwithstanding the delay, the biofilm density required for *phzA* activation was ~9-fold lower under P-
241 lim than P-rep (constitutive reporter [a.u.]: P-lim 27,852 ± 1,207; P-rep 248,856 ± 13,115; mean ± SD),
242 which is consistent with planktonic trends.

243 2 mL agar: Under P-lim, *phoA* was, again, detected early (~9.5 hr), *phzA* induction occurred (~18 hr;
244 earlier than 5 mL condition), and before P-rep (~20 hr), suggesting that QS-signal thresholds were

245 achieved more rapidly when sink capacity was reduced (i.e., lower agar volume). Interestingly, the
246 biofilm density at the time of *phzA* induction was nearly identical between the 2 mL and 5 mL conditions,
247 for both P-lim and P-rep, indicating that biomass accumulation was faster under 2 mL, likely contributing
248 to the earlier induction. Lastly, as in the 5 mL agar experiments, P-lim, again, required ~10-fold lower
249 cell density than P-rep for *phzA* activation.

250 The addition of exogenous AHL caused P-lim colonies to induce *phzA* expression rapidly, coincident with
251 the onset of phosphorus stress and bypassing the need for signal accumulation through growth. AHL
252 rescue in P-rep colonies also accelerated the induction time but still required a higher cell density than P-
253 lim. This is again consistent with liquid cultures. Exogenous AHL accelerated induction but did not
254 bypass the requirement for phosphorus limitation or a high biofilm density.

255 Together, these results show that QS activation in colony biofilms reflects an interplay between nutrient
256 status and the balance of AHL signal accumulation versus diffusive loss in the surrounding agar.
257 Phosphorus limitation lowers the biofilm density required for QS activation, but induction still depends
258 on local signal concentration, which is influenced by retention within the biofilm versus loss into the agar.

259 **Phosphorus stress and spatial confinement accelerate quorum sensing in soil-like**
260 **microenvironments**

261 To examine how the physical structure of the environment shapes local signal accumulation and QS
262 activation, we used a previously designed microfluidic platform that mimics soil-like porous media[64] (Fig.
263 4A). Low-density cultures (OD_{600} = 0.05) of a dual reporter strain (*P. synxantha* 2-79 P_{tac}-P_{phzA}) were
264 inoculated and air was introduced to generate a landscape of water pockets that varied in size,
265 connectivity, saturation levels (Fig. 4B). Across roughly 50 regions of interest (ROIs) imaged in each
266 experiment, we tracked biomass (P_{tac}) and *phz* induction (P_{phzA}) (Fig. 4C, Fig. S2).

267 Comparing P-lim and P-rep conditions revealed that phosphorus stress strongly advanced QS activation
268 and lowered the biomass required for *phz* induction (Fig. 4D,E). Under P-lim, ROIs typically induced
269 within a few hours (mean induction time ~5 hr) and did so at relatively low biomass, whereas under P-rep
270 conditions induction was markedly delayed (mean ~32 hr) and required substantially higher biomass at
271 the time of activation (on average 5-fold greater intensity). Induction times were also much more
272 heterogeneous across ROIs under P-rep conditions. Because this reactor is not well mixed, additional
273 transport and resource gradients almost certainly emerge that affect the observed timing that we do not
274 control for (e.g., oxygen depletion in larger pores). In this more realistic geometry, the contrast between
275 P-lim and P-rep induction time appears amplified relative to previous experiments (Figures 2 and 3).

276 We next asked whether QS induction under P limitation depends on initial cell density within individual
277 water pockets. To quantify this feature, we used the ratio of cell area to water area at t = 1 hr for each ROI
278 as a metric for initial cell density and related it to the time of *phz* induction for each ROI. Across P-lim
279 experiments, induction time decreased systematically with increasing starting density, following a non-
280 linear, approximately power-law relationship ($R^2 = 0.65$, Fig. 4F, Fig. S3). Pearson and Spearman
281 correlations gave similar results ($r = -0.771$, $p = 4.14e-20$; $\rho = -0.839$, $p = 1.59e-26$). Therefore, most of
282 the variation in induction timing is explained by initial cell density, supporting a view in which
283 phosphorus stress and spatial confinement allow cells concentrated in pore water to accelerate phosphate
284 depletion and AHL accumulation to facilitate QS activation.

285 Taken together, these data demonstrate that the combination of phosphorus stress and spatial confinement
286 enables QS activation in microenvironments that would otherwise restrict signal buildup. We next asked
287 whether lowered QS concentration thresholds could provide an ecological advantage in a community
288 setting.

289

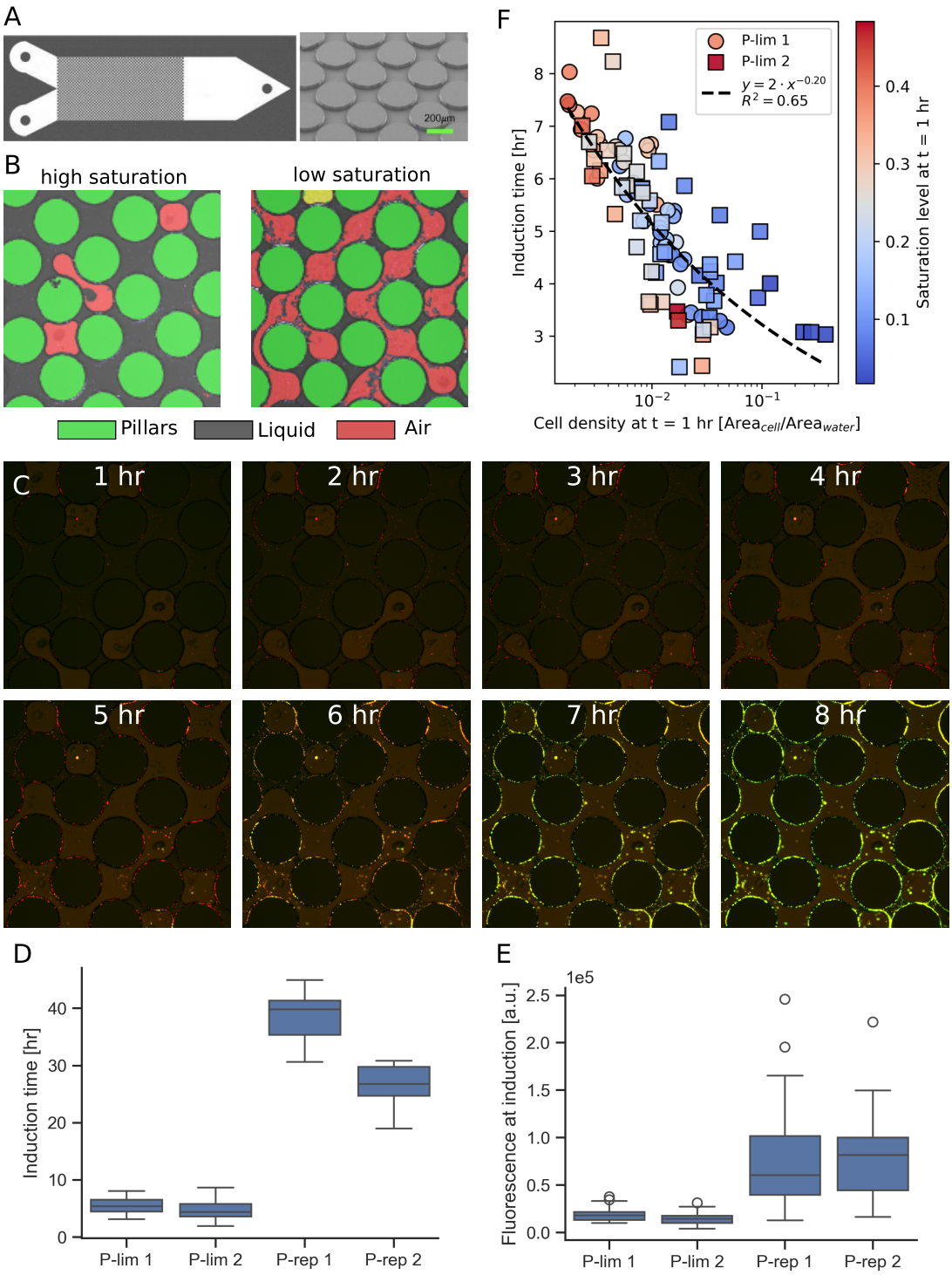

Figure 4: Relationship between cell density, water saturation, and *phz* induction time in microfluidic microenvironments. (A) Schematic (left) and scanning electron micrograph (right) of the synthetic porous platform used to create spatially structured microenvironments. The reactor consists of a 2 by 1 cm pore network containing an array of evenly spaced cylindrical posts 300 μm in diameter, a

295 depth of 10 µm, and a porosity of 0.39. **(B)** Representative images of pore-scale water distribution at high
296 saturation and low saturation levels, with pillars shown in green, water-filled pores in gray, and air-filled
297 pores in red. **(C)** Representative composite images of reporter induction (constitutive: red, *phzA*: green)
298 over time. **(D)** Boxplots summarizing *phz* reporter induction times for individual ROIs across replicate P-
299 lim (P-lim 1–2) and P-rep (P-rep 1–2) experiments. Boxes show medians and interquartile ranges;
300 whiskers extend to 1.5× the interquartile range. See Figure S2 for induction time estimation. **(E)** Boxplots
301 summarizing red-channel integrated fluorescence per ROI (density proxy) at the time of *phz* reporter
302 induction across replicate P-lim (P-lim 1–2) and P-rep (P-rep 1–2) experiments. Boxes show medians and
303 interquartile ranges, and whiskers extend to 1.5× the interquartile range. **(F)** Distribution of induction
304 times under P-lim. Relationship between cell density in pore water (x-axis; area fraction of cells in water-
305 filled regions at t = 1 hr) and *phz* induction time (y-axis) for P-lim 1 (circles) and P-lim 2 (squares). Points
306 are colored by water saturation (fraction of pore volume filled with water), as indicated by the color bar.
307 The dashed line shows a power-law fit to all data. Data represent pooled technical replicates from regions
308 in the reactor (P-lim 1, n = 44 ROIs; P-lim 2, n = 52 ROIs).

309

310 **Phosphorus limitation confers cooperative and antagonistic quorum-sensing-driven community**
311 **dynamics**

312 Under nutrient stress, microbial communities can flip between cooperative information exchange (e.g.,
313 quorum signals) and antagonistic interference (e.g., antibiotics), reshaping which partners win or lose.

314 To determine whether phosphorus limitation broadly enhances AHL production and promotes cross-talk
315 among *Pseudomonas* species, we assembled a panel of rhizosphere-associated strains representing both
316 close relatives of *P. synxantha* and more distantly related pseudomonads. Each strain was grown under N-
317 lim, P-lim, or P-rep conditions, cell-free supernatants were then collected to challenge the *P. synxantha*
318 Δ*phzI*–P_{phzA} reporter, which cannot synthesize AHLs but fluoresces upon QS-activated *phzA* expression
319 (Fig. 5A). Supernatants from multiple donors activated the reporter, with the strongest and broadest
320 induction under P-lim and P-rep, and little to none under N-lim. As expected, controls with the Δ*phzI*
321 donor did not induce, whereas the wild-type donor triggered a robust response. Notably, across the panel,
322 strains carrying homologous *phzIR* operons consistently induced *phzA* under P-lim, suggesting that
323 phosphorus stress broadly elevates AHL output among *Pseudomonas* species. In contrast, *P. aeruginosa*

PA14 failed to induce the reporter, consistent with its production of 3-oxo-acyl-HSLs rather than the 3-hydroxy-acyl-HSL(s) recognized by PhzR in *P. synxantha*.

Next, we asked whether QS activation under P-lim alters microbial interactions within competitive communities under oxic conditions where phenazines primarily function as antibiotics.[11] We performed co-culture assays between *P. synxantha* (wild type and Δ*phzA-G*, a phenazine-null mutant) and *Pedobacter kyonggii*, a common rhizosphere isolate. When P-limited, the wild-type strain significantly suppressed *P. kyonggii* growth, whereas the Δ*phzA-G* mutant did not (Fig. 5B). This phenazine-linked advantage was absent under N-lim in the wild-type strain and, interestingly, under P-rep conditions as well. Although the wild type produced PCA under P-replete conditions, induction occurred much later (~35 h vs ~16 h in P-lim; see Fig. S5), by which time the co-cultures had already completed most of their growth, leaving little opportunity for inhibition to manifest. Thus, the phenotype likely reflects the timing of phenazine onset relative to culture growth.

These findings indicate that phosphorus limitation broadly elevates AHL signaling across *Pseudomonas* spp., priming QS in *P. synxantha*. Moreover, phenazine production under phosphorus stress suppresses growth of *P. kyonggii*.

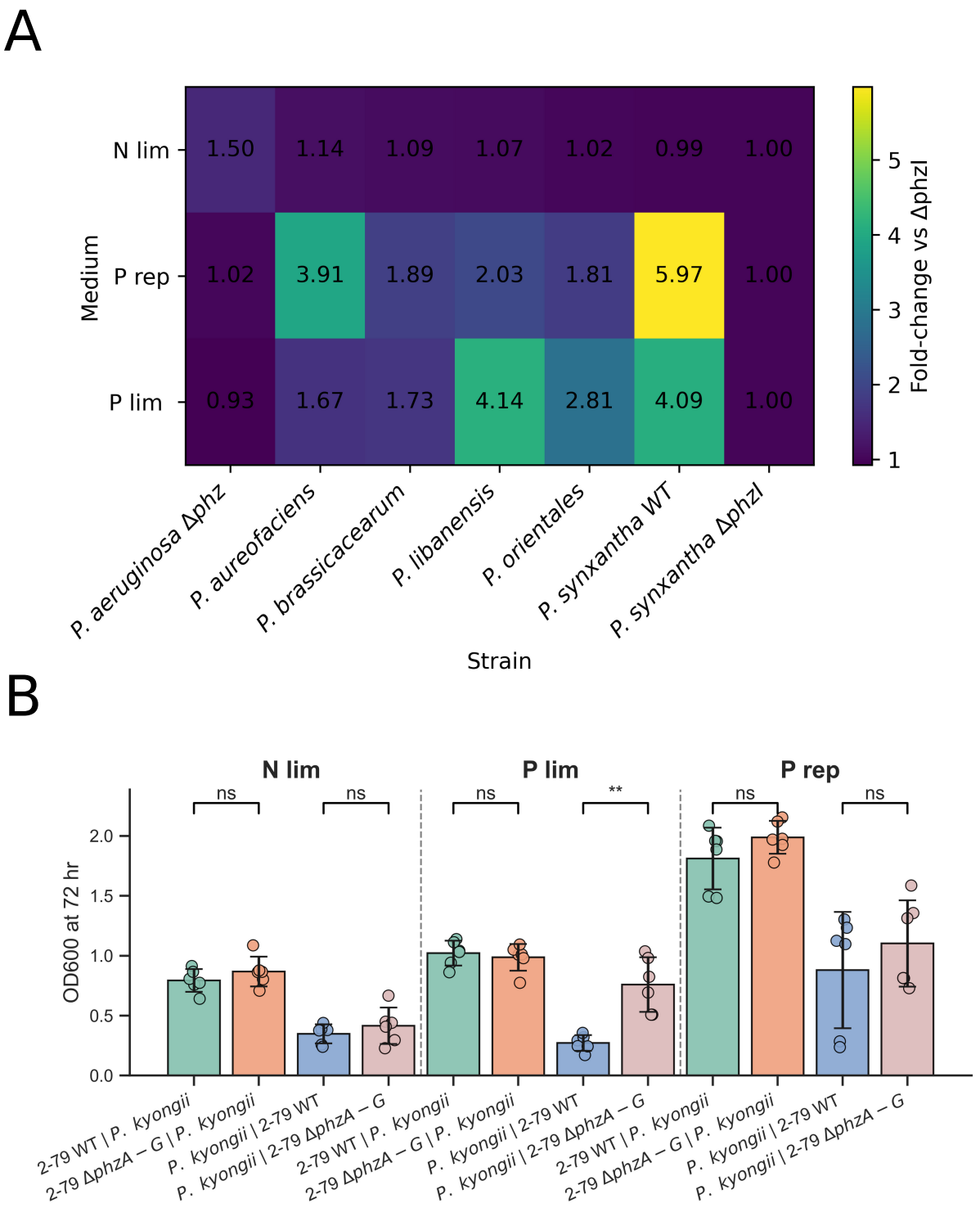

Figure 5: (A) *Pseudomonas* spp. supernatant cross-induction QS assay. Heatmap of fluorescence induction in *P. synxantha* Δ*phzI*-P_{phzA} across supernatants of selected strains and media conditions at 24 h. Rows represent media (N-lim, P-lim, P-rep); columns are strain supernatants. Each cell shows the fold-

343 change of the chosen metric relative to the reference strain, *P. synxantha* Δ*phzI*, within the same medium.
344 Where shown, numeric labels are fold-change values rounded to two decimals; the *P. synxantha* Δ*phzI*
345 column equals 1 by definition. Fluorescence is normalized by OD600. (mean, $n = 6$) **(B) Competition**
346 **assays between *P. synxantha* against *Pedobacter kyonggii* under various nutrient regimes**. Bar plots
347 show OD600 at 72 h (mean ± SD, $n = 6$) for four pairings. The first name indicates the strain measured;
348 the second is its pairing partner. Results are shown separately for N-lim, P-lim, P-rep media. *P. synxantha*
349 wild type (2-79 WT) and *P. synxantha* Δ*phzA-G* (2-79 Δ*phzA-G*). Statistical comparisons use Welch's *t*-
350 test; brackets denote significance (ns, not significant; ** $p < 0.01$).

351

352 **Discussion**

353 Our study reveals that phosphorus limitation rewires the quorum-sensing (QS) circuitry of *Pseudomonas*
354 *synxantha* 2-79, lowering the effective signal concentration required for autoinduction and enabling
355 phenazine biosynthesis at conditions corresponding to much lower densities (OD ≈ 0.08 in liquid
356 cultures). Phosphorus stress reduces the acyl-homoserine lactone (AHL) concentration required for
357 activation by roughly an order of magnitude under our tested conditions, thereby heightening cellular
358 sensitivity to QS signals. This response depends on the PhoBR two-component system: inactivation of
359 PhoBR abolishes phenazine induction even when AHL levels are high, demonstrating that phosphorus
360 stress provides a necessary regulatory input. In structured habitats, where mass transfer alters QS
361 molecule accumulation, phosphorus limitation emerges as a key modulator of QS activation. In colony
362 biofilms, phenazine induction times under P limitation are strongly affected by agar volumes and biofilm
363 density, implicating biofilm retention and diffusive losses in achieving threshold AHL concentrations.
364 Exogenous AHL addition collapses this concentration requirement but still requires a physiological state
365 primed for induction (i.e., P limitation or higher cell densities under P replete). Confinement in
366 micropores creates microenvironments that retain signals and enable localized QS activation, again
367 showing that physical structure and nutrient state jointly set QS thresholds. These environmentally-tuned
368 threshold shifts have ecological consequences. Under phosphorus limitation, *P. synxantha* inhibits growth
369 of the rhizosphere isolate *Pedobacter kyonggii* through phenazine production, a benefit lost in the
370 phenazine-null mutant and under nitrogen limitation or phosphorus-replete conditions. Early phenazine

371 synthesis may thus serve dual functions in resource competition and phosphorus acquisition, coordinated
372 through stress-responsive signaling.

373 Our data argue against "concentration-only" or "density-only" views and instead support an AND-gate
374 model for QS activation: (i) sufficient signal accumulation (production versus diffusion, advection,
375 sorption, and decay) to cross a threshold and (ii) a physiological readiness state that licenses
376 responsiveness. Density remains a useful proxy because per-cell production scales with biomass and high
377 density often coincides with a physiological readiness, but other regulatory programs can shift the
378 effective threshold, explaining low-density induction under nutrient stress. In our system, QS signal
379 responsiveness is tunable by nutrient status, PhoBR under phosphorus limitation, so signal is necessary
380 but not sufficient. This framework reconciles our observations: under P-replete + excess AHL, low-
381 density cultures fail to induce despite ample signal, indicating physiological unreadiness; responsiveness
382 emerges by mid- to late-exponential growth as global regulators (e.g., Gac/Rsm) and stress programs rise.
383 Under P limitation, induction synchronizes with phosphorus stress. Exogenous AHL enables induction at
384 comparatively lower cell densities, with the activation density tunable by the imposed Pi level. Again,
385 though, induction did not occur until P limitation was achieved.

386 This model aligns with prior work. Overactivation of the stringent response via RelA in *P. aeruginosa*
387 prematurely activates RpoS, LasR, RhlR and autoinducer synthesis, driving LasB production independent
388 of density, i.e., physiological readiness upstream of signal thresholds.[65] Exogenous PQS (an autoinducer)
389 addition can override cell-density dependence but not growth-phase dependence, underscoring the
390 physiological readiness requirement.[66] More broadly, nutrient limitation and growth rate jointly modulate
391 extracellular signal accumulation across species, with phosphorus and sulfur limitation disproportionately
392 elevating alkylquinolones even at lower OD.[67] Our findings extend this signal-accumulation +
393 physiological readiness concept by showing that native PhoBR directly sensitizes an unmodified AHL-
394 based QS network in a rhizosphere pseudomonad, reframing QS as an environmentally tuned
395 concentration-sensing mechanism whose effective activation threshold is set jointly by autoinducer

concentration and regulatory state. Related frameworks[43] reach similar conclusions; nevertheless, proliferating new labels for QS risks semantic confusion that can imply a single dominant driver.[36] Instead, we favor a generalizable AND-gate view that explains QS outputs in sparse, fragmented soils and highlights practical levers (e.g., nutrient availability, confinement, and mass transfer) for engineering compatible microbial communities and biosensors in heterogeneous environments.

Methods:

Bacteria. The primary strain was *Pseudomonas synxantha* (formerly *P. fluorescens*) 2-79 WT. Isogenic derivatives included Δ*phzI* (AHL synthase null), Δ*phzA-G* (phenazine-null), and Δ*phoB* (phosphorus-stress response regulator null). Reporters carrying transcriptional fusions included P_{phzA}–mNeonGreen (QS/phenazine biosynthesis), P_{phoA}–mNeonGreen (phosphorus stress), P_{phzA}–GFP, P_{tac}–mCherry (QS/phenazine biosynthesis, density metric) and $P_{PA10403}$-mNeonGreen (density metric). Donor/competitor strains for crosstalk and competition assays included *Pseudomonas aureofaciens* 30-84, *P. brassicacearum* 106, *P. libanensis* 84, *P. orientalis*, *P. aeruginosa* Δ*phz1/2* and *Pedobacter kyonggii*. Sources, identifiers, and genotypes are listed in Table S2.

Culture conditions. Unless noted, overnight cultures of *Pseudomonas* strains were propagated at 30 °C, 250 rpm in LB (Miller) for 16-18 h; *E. coli* DH10B/SM10 were grown at 37 °C. Experimental assays used defined MOPS medium (below). Antibiotics were used only for selection (gentamicin 30 μg mL^{-1}, tetracycline 15 μg mL^{-1}). All experiments with reporters were antibiotic-free. Strains were stored as −80 °C glycerol stocks (20% v/v) and streaked fresh for each experiment.

Media compositions and nutrient-regime definitions

MOPS defined medium. Per liter: 25 mM MOPS (pH 7.0; adjusted with 1 M NaOH), 55.5 mM glucose, 16 mM NH_4Cl, 7 mM KH_2PO_4, 0.41 mM $MgSO_4 \cdot 7H_2O$, 0.68 mM $CaCl_2 \cdot 2H_2O$, Aquil-based trace metals[68] with Fe 10 μM and EDTA 100 μM. KH_2PO_4 7 mM (P-rep/N-lim) or 25–100 μM (P-lim); NH_4Cl

419 16 mM (P-rep/P-lim) or 2 mM (N-lim). No-N and No-N/P buffers omitted NH_4Cl and NH_4Cl/KH_2PO_4,
420 respectively. MOPS agar consisted of MOPS medium with 1.0% (w/v) noble agar.
421 **Plant medium.** 0.5× MS (Sigma-Aldrich M5519), 0.6% (w/v) Phytagel (Sigma-Aldrich P8169), pH 5.8
422 (KOH); P-lim omits KH_2PO_4.
423 **Phosphate-sorbing (P-HFO) condition.** Hydrous ferric oxide (HFO) was synthesized, phosphate was
424 then sorbed and sequestered (P-HFO). P-HFO was added to phosphorus deficient plant medium (see
425 below) at 1.6 g/L. See Note S1 for P-HFO preparation.
426 **MES defined medium.** Per L: 50 mM MES pH 5.8 (KOH), 50 mM sucrose, salts as above. KH_2PO_4 7
427 mM (P-rep/N-lim) or 100 µM (P-lim); NH_4Cl 16 mM (P-rep/P-lim) or 2 mM (N-lim).

428 **Reporter and mutant generation and verification**

429 Transcriptional fusions were constructed using the mini-Tn7 system.[69] Promoter (P_{phzA}) was cloned
430 upstream of mNeonGreen in pJM220 by Gibson assembly and transformed into *E. coli* DH10B.
431 Gentamicin-resistant transformants (30 µg mL^{-1}) were verified by colony PCR and Sanger sequencing.
432 Mini-Tn7 elements and pTNS1 helper (TnsABCD; delivered from *E. coli* SM10/pTNS1) were introduced
433 into electrocompetent *P. synxantha* 2-79. Transconjugants were selected on LB-gentamicin and screened
434 by junction PCR for single-copy insertion at attTn7 (downstream of *glmS*). Reporter function was
435 validated in plate-reader assays (P_{phzA} induction under QS-permissive conditions). Plasmids and primers
436 are listed in Tables S3–S4.

437 In-frame deletion mutants were constructed using a suicide plasmid. Approximately 1-kb regions
438 upstream and downstream of *phzA-G* and *phzI* were PCR-amplified and assembled with SmaI-digested
439 pEX18Gm by Gibson assembly. The plasmid was electroporated into *E. coli* DH10B, and transformants
440 were selected on LB agar with gentamicin (30 µg mL^{-1}). Correct constructs were verified by PCR and
441 introduced into *P. synxantha 2-79* wild-type strains via triparental conjugation. Merodiploids were
442 selected on Vogel–Bonner minimal medium (VBMM) containing gentamicin (30 µg mL^{-1}), followed by

443 counter-selection on sucrose medium (5 g L^{-1}yeast extract, 10 g L^{-1}tryptone, 100 g L^{-1}sucrose). Colonies
444 in which homologous recombination was successful were identified by PCR. Deletions were confirmed
445 by diagnostic PCR across the targeted loci and by phenotype: Δ*phzA-G* lacked ABS367nm (PCA readout)
446 signal and lacked phenazine product, verified via LC-MS analysis. Δ*phzI* required exogenous AHL for
447 induction and lacked AHL production, verified via LC-MS/MS analysis.

448 **Plant-microbe reporter induction assay**

449 *Brachypodium distachyon* Bd21-3 seeds were dehusked, sterilized with chlorine gas (see Note S2), plated
450 on 0.6% Phytagel with 0.5× MS, and vernalized (4 °C, 4 d). Seedlings were grown 2 d (16 h light/8 h
451 dark, 25 °C), then immersed 30 min in 0.5× MS lacking phosphate (P-lim) containing *P. synxantha* 2-79
452 at OD_{600} = 0.1. Seedlings were transferred into 1 cc syringes filled with 0.6% Phytagel prepared with 0.5×
453 MS under the indicated phosphorus condition (P-lim, P-rep, or P-HFO) and incubated vertically for 2 d
454 prior to imaging.

455 Seedlings embedded in phytagel were mounted so that roots+phytagel were submerged in sterile 0.5× MS
456 buffer. Imaging used a Zeiss Lightsheet Z.1 with EC Plan-Neofluar 5×/0.16 air objective. Dual-channel
457 acquisition captured GFP/mNeonGreen (488 nm ex, 498 nm em) and mCherry (561 nm ex, 571 nm em)
458 on separate cameras with a dual-band emission filter (Zeiss LBF 488/561). Z-stacks were collected at 5
459 µm step, XY pixel 0.93 µm, 100 ms exposure per slice; laser power was held constant across conditions
460 (20% at 488 and 561 nm). Maximum intensity projections (MIPs) were generated for analysis.

461 All analysis used Fiji/ImageJ with a custom macro. Red channel (P_{tac}–mCherry) was median-filtered (r =
462 4), background-subtracted (rolling ball 50 px), converted to 8-bit, and locally thresholded (Bernsen, r =
463 15) to build masks. Objects were defined by particle analysis (min size 20 px) and applied to original
464 red/green images to extract integrated density (IntDen) and area. Mean intensity per object was computed
465 as IntDen/area for both channels. CSVs were exported for Python analysis.

466 **Planktonic 96-well kinetic experiments**

467 Overnight cultures of *P. synxantha* 2-79 (WT, Δ*phzA-G*, Δ*phzI*, Δ*phoB,* Δ*phzI*–P_{phzA}) were washed 3× in
468 MOPS containing 10 µM phosphate, and inoculated into 96-well plates at OD_{600} = 0.01. Plates were
469 incubated in a Tecan Spark 10M (30°C; orbital shaking amplitude 2.5 mm, 216 rpm) with reads every 15
470 min for 24 h. OD_{600} was read at 600 nm; ABS367 was read at 367nm for PCA-associated absorbance;
471 mNeonGreen at Ex/Em 485/535 nm. Induction time was approximated from fluorescence time series by
472 manual curation. ODs at induction were obtained by linear interpolation of OD_{600} (t) at that time.

473 For the AHL-supplemented dose-response assays, 3-OH-C6-HSL (Adipogen; ≥98%) stock was prepared
474 with methanol (final solvent ≤0.02% v/v; vehicle controls showed no effect from solvent carryover). Dose
475 ranges spanned sub-nM to tens of µM (specified per figure).

476 For the no-growth supplementation assay, Δ*phzI* overnight culture was washed (3×) in the respective
477 treatment buffer (No-N or No-N/P) were inoculated at OD_{600} = 0.1. For the growth-permissive
478 supplementation assays, Δ*phzI* overnight culture was washed (3×) in MOPS containing 10 µM phosphate
479 and inoculated at OD_{600} = 0.01. Responses were baseline-corrected to 0 µM within condition and fit with
480 a two-parameter Hill (log-logistic) model (top = 1, bottom = 0) to estimate EC_{50} with 95% CIs.

481 **AHL quantification by LC–MS/MS**

482 Overnight cultures of *P. synxantha* 2-79 (WT, Δ*phzI*) were washed 3× in MOPS, then grown in glass
483 culture tubes (30 °C, 250 rpm) under P-rep, P-lim, and N-lim conditions for 22 h. Cultures were then
484 pelleted, supernatants were collected, filtered through a 0.22 µm PES filter, diluted 1:1 in methanol,
485 incubated for 1 h at -20°C, pelleted, then supernatants were collected before analyzing.

486 Analytical standards (3-OH-C6-HSL, 3-OH-C8-HSL, 3-OH-C10-HSL, and 3-oxo-C8-HSL; ≥95–98%
487 purity; Adipogen/Cayman) were prepared by solubilizing powders in methanol as 1-10 g L^{-1} primary

488 frozen stocks (-20 °C). A 100 µM all analyte mix was made in methanol with 0.1% formic acid.
489 Calibration standards were prepared by diluting the analyte mix in methanol with 0.1% formic acid.

490 A Waters (Milford, MA) Acquity Premier UPLC was fitted with a HSS T3 column and coupled to a Xevo
491 Q-TOF G2S. Mobile phase A was 0.1% formic acid in water and mobile phase B was 100% acetonitrile.
492 The initial mobile phase composition was 2.5 % B for 0.5 minutes with a linear gradient to 95% B ending
493 at 5 minutes. After a 0.5 minute hold (5.5 min) the composition was returned rapidly to the initial
494 conditions (5.6 min) and held for an additional 0.25 minutes (to 5.74 minutes). The gradient was cycled
495 without interruption during any acquisition. The flow rate was held constant throughout at 0.3 mL/min,
496 the samples held at 10 °C, the column temperature maintained at 40 °C, and the injection volume was 4
497 µL. The 2.1 mm × 50 mm × 1.8 µm column was used without a guard column.

498 The ion source block was held at 120 °C, capillary voltage was 3 kV, desolvation gas flow and
499 temperature were 600 lph and 500 °C, the cone gas flow as 15 lph, and the source offset was 80 V.
500 Separate mass spectral data sets were collected in both MS mode from 50-1200 m/z and using scheduled
501 MS2 for parallel reaction monitoring of the individual targeted analytes. MS data was acquired in positive
502 sensitivity mode (approximately 18,000 resolution). The mass axis was calibrated against sodium formate
503 and was confirmed daily. Leucine enkephalin was used as lock mass reference during acquisition.

504 Targeted analysis was performed using the Quanlynx program within the Masslynx software suite used to
505 operate the instrument.

506 **Sessile early-stage colony biofilm experiments**

507 Overnight cultures of *P. synxantha* 2-79 (WT, P_{phoA}, P_{phzA}, $P_{PA10403}$) were washed 3× in MOPS containing
508 7 mM phosphate and adjusted to OD_{600}= 0.05. A 5 µL droplet was spotted onto agar plates, air-dried 1 h,
509 and placed in a custom humidity-controlled platform. The agar plates contained either 2 mL or 5 mL of
510 agar. For P-lim plates, phosphorus was omitted from the MOPS agar; the only source of phosphorus was

511 the 5 μL inoculation drop that contained 7 mM phosphate. P-rep consisted of MOPS agar at 7 mM.
512 Images were acquired hourly for 36 h.

513 Time-lapse imaging of bacteria was performed using a previously reported complex-field and
514 fluorescence microscopy system based on the aperture scanning technique (CFAST).[48] Samples were
515 mounted in a 12-well plate and positioned on a motorized XY scanning stage (Thorlabs MLS203-1) to
516 enable automated, parallel scanning of multiple wells.

517 To minimize evaporation of the growth medium during the two-day imaging experiments, the 12-well
518 plate was placed in a custom 3D-printed holder containing wet paper towels to maintain high local
519 humidity. To maintain focus while minimizing photobleaching and phototoxicity, 0.5-μm red fluorescent
520 beads (580/605 nm, ThermoFisher F8812) were pre-mixed with the bacterial suspension at a $1:10^5$
521 dilution from stock. These beads served as markers for focal plane tracking. The beads were excited with
522 a 568 nm laser (Coherent Sapphire 568 LP), and the emitted fluorescence was filtered using a dichroic
523 mirror (Semrock Di01-R488/561) and a bandpass filter (Semrock FF01-R523/610).

524 A 488 nm laser (Thorlabs LP488-SF20G) was used both for complex-field illumination and for excitation
525 of mNeonGreen fluorescence. The complex field data comprising both amplitude and quantitative
526 phase was used to quantify the area coverage of bacterial colonies. Fluorescence intensity was extracted
527 from the mNeonGreen images and subsequently normalized using brightfield images to compensate for
528 variations in excitation power due to differences in medium thickness across the sample.

529 **Microfluidic soil-analog reactor experiments**

530 Devices followed a silicon-etched porous design[64] and fabrication process (see Note S3). Overnight
531 culture of *P. synxantha* 2-79 (dual reporter, P_{phzA}-P_{tac}) was washed 3× in MOPS P-lim (100 μM) or P-rep
532 medium and adjusted to OD_{600}= 0.05 for inoculation into the reactor. Cells were inoculated at a flow rate
533 of 0.1 mL min^{-1} for 3 minutes. Air was then injected and generated heterogeneous water saturation

534 (connected high-saturation domains vs confined pockets). After initial displacement, air was continuously
535 injected at a flow rate of 0.01 mL min^{-1}. Imaging was conducted for 16-40 h depending on experiment.

536 All imaging was performed on a Nikon Ti2 widefield epifluorescence microscope. Time-lapse series used
537 a Plan Apo 20×/0.75 dry objective. GFP was excited with a 488-nm LED and collected with a FITC filter
538 set; mCherry was excited with a 561-nm LED and collected with a TRITC filter set. Images were
539 collected every hour from multiple stage positions.

540 Custom MATLAB code was used to segment bacterial cells based on the red channel (constitutive
541 reporter) and pockets of air based on the green channel (induction of phenazine production). To identify
542 cells, background subtraction was applied to the original image followed by thresholding using a fixed
543 intensity value. Objects smaller than 5px were discarded. To segment pockets of air, we first identified
544 and removed signal from induction, which would otherwise interfere with the detection. For this we
545 segmented fluorescing cells by simple thresholding, expanded their area by dilation (10px) and then
546 replaced intensity values within this area with the background intensity. Following this, air pockets were
547 segmented by smoothing and background subtraction followed by thresholding. Areas smaller than
548 1000px were discarded and holes within air pockets smaller than 50000px were closed. When necessary,
549 segmentation of air pockets was corrected manually. Intensity ratios were based on background-corrected
550 intensities. Induction time vs cell density was fit to a power-law model using log–log linear regression;
551 goodness-of-fit (R^2) and CI on parameters are reported.

552 **Supernatant cross-induction assay**

553 Overnight cultures of *Pseudomonas* strains were washed 3× in MOPS (P-lim and N-lim) medium and
554 inoculated at OD_{600} =0.01 into glass culture tubes (30 °C, 250 rpm) under P-rep, P-lim, and N-lim
555 conditions for 22 h. Cultures were then pelleted, and supernatants were collected and filtered through a

556 0.22 µm PES filter. The cell-free supernatant was then mixed 1:1 with appropriate medium (i.e., P-rep, P-
557 lim, N-lim) for cross-induction assay.

558 An overnight culture of *P. synxantha* 2-79 Δ*phzI*-P_{phzA} was washed 3× in MOPS (P-lim and N-lim) and
559 inoculated at OD_{600} =0.01. A 96-well plate assay was then conducted with the cell-free supernatant
560 mixture following the "Planktonic 96-well kinetic experiments" parameters. Fold-change for RFU/OD_{600}
561 relative to the reference strain *P. synxantha* Δ*phzI* within each medium was then computed. The resulting
562 scores were plotted as a single heatmap.

563 **Pairwise competition assays**

564 Co-culture growth and induction dynamics were monitored using a two-chamber co-culture system that
565 allows fluidic exchange while physically separating populations (Duet Co-Culture System, Cerillo). *P.*
566 *synxantha* (WT or Δ*phzA-G*) and *P. kyonggii* overnight cultures were washed 3× in MES (P-lim and N-
567 lim) medium. Cells were then loaded to either side of the chamber at a starting OD_{600} of 0.01 under N-lim,
568 P-lim, or P-rep media. Duets have the footprint of a 96-well plate, thus the assay was conducted following
569 "Planktonic 96-well kinetic experiments" instrument parameters. Phenazine-dependent suppression was
570 assessed by comparing WT vs Δ*phzA-G*. Statistics used Welch's t-test with two-sided $\alpha = 0.05$. Note that
571 competition assays were run in MES-defined medium (pH 5.8) with sucrose as the carbon source. Sucrose
572 was chosen because *P. synxantha* 2-79 does not utilize it; on glucose, *P. synxantha* rapidly overgrows
573 *Pedobacter kyonggii*, obscuring interaction effects. Using sucrose maintains competitive viability of *P.*
574 *kyonggii* and shifts *P. synxantha* toward relying on metabolites released by P. *kyonggii*, enabling
575 resolution of phenazine-dependent outcomes. The pH was set to 5.8 (buffered with MES) to approximate
576 mildly acidic rhizosphere conditions and because PCA is more membrane-permeant—and thus more
577 potent—at lower pH.

Acknowledgements:

We acknowledge the Resnick Ecology and Biosphere Engineering Facility and Caltech Biological Imaging Center for the training and use of confocal and light sheet fluorescence microscopes. We are grateful to the Resnick Sustainability Institute and National Institute of Health (2R01AI127850-06A1) for enabling resources and financial support. R.E.A. was supported by an NSF Postdoctoral Research Fellowship in Biology (Grant No. 2209379). H.J. was supported by a Helen Hay Whitney Postdoctoral Research Fellowship.

Author contributions: R.E.A., and D.K.N. designed research; R.E.A., H.J., O.Z., R.L.A., and N.D. performed research; R.E.A., H.J., O.Z., R.L.A., and N.D. analyzed data; and R.E.A., H.J., O.Z., R.L.A., N.D., D.M., C.Y., and D.K.N. wrote the paper.

References:

1. Mavrodi, D.V., Blankenfeldt, W., Mavrodi, O.V., Weller, D.M., and Thomashow, L.S. (2025). Microbial phenazines: biosynthesis, structural diversity, evolution, regulation, and biological significance. Microbiology and Molecular Biology Reviews *0*, e00147-23. https://doi.org/10.1128/mmbr.00147-23.

2. Dahlstrom, K.M., McRose, D.L., and Newman, D.K. (2020). Keystone metabolites of crop rhizosphere microbiomes. Current Biology *30*, R1131–R1137. https://doi.org/10.1016/j.cub.2020.08.005.

3. Zhou, Y., Wang, H., Sun, J., Wicaksono, W.A., Liu, C., He, Y., Qin, Y., Berg, G., Li, L., Lin, H., et al. (2025). Phenazines contribute to microbiome dynamics by targeting topoisomerase IV. Nat Microbiol *10*, 2396–2411. https://doi.org/10.1038/s41564-025-02118-0.

4. Dar, D., Thomashow, L.S., Weller, D.M., and Newman, D.K. (2020). Global landscape of phenazine biosynthesis and biodegradation reveals species-specific colonization patterns in agricultural soils and crop microbiomes. eLife *9*, e59726. https://doi.org/10.7554/eLife.59726.

5. Menezes-Blackburn, D., Giles, C., Darch, T., George, T.S., Blackwell, M., Stutter, M., Shand, C., Lumsdon, D., Cooper, P., Wendler, R., et al. (2018). Opportunities for mobilizing recalcitrant phosphorus from agricultural soils: a review. Plant Soil *427*, 5–16. https://doi.org/10.1007/s11104-017-3362-2.

6. McRose, D.L., and Newman, D.K. (2021). Redox-active antibiotics enhance phosphorus bioavailability. Science *371*, 1033–1037. https://doi.org/10.1126/science.abd1515.

610 7. Cox, C.D. (1986). Role of pyocyanin in the acquisition of iron from transferrin. Infection and
611 Immunity *52*, 263–270. https://doi.org/10.1128/iai.52.1.263-270.1986.

612 8. Hernandez, M.E., Kappler, A., and Newman, D.K. (2004). Phenazines and other redox-active
613 antibiotics promote microbial mineral reduction. Appl Environ Microbiol *70*, 921–928.
614 https://doi.org/10.1128/AEM.70.2.921-928.2004.

615 9. Wang, Y., Wilks, J.C., Danhorn, T., Ramos, I., Croal, L., and Newman, D.K. (2011). Phenazine-1-
616 Carboxylic Acid Promotes Bacterial Biofilm Development via Ferrous Iron Acquisition. Journal of
617 Bacteriology *193*, 3606–3617. https://doi.org/10.1128/jb.00396-11.

618 10. LeTourneau, M.K., Marshall, M.J., Grant, M., Freeze, P.M., Strawn, D.G., Lai, B., Dohnalkova,
619 A.C., Harsh, J.B., Weller, D.M., and Thomashow, L.S. (2019). Phenazine-1-Carboxylic Acid-
620 Producing Bacteria Enhance the Reactivity of Iron Minerals in Dryland and Irrigated Wheat
621 Rhizospheres. Environ. Sci. Technol. *53*, 14273–14284. https://doi.org/10.1021/acs.est.9b03962.

622 11. Price-Whelan, A., Dietrich, L.E.P., and Newman, D.K. (2006). Rethinking "secondary" metabolism:
623 physiological roles for phenazine antibiotics. Nat Chem Biol *2*, 71–78.
624 https://doi.org/10.1038/nchembio764.

625 12. Meirelles, L.A., and Newman, D.K. (2018). Both toxic and beneficial effects of pyocyanin contribute
626 to the lifecycle of Pseudomonas aeruginosa. Molecular Microbiology *110*, 995–1010.
627 https://doi.org/10.1111/mmi.14132.

628 13. Perry, E.K., and Newman, D.K. (2022). Prevalence and Correlates of Phenazine Resistance in
629 Culturable Bacteria from a Dryland Wheat Field. Applied and Environmental Microbiology *88*,
630 e02320-21. https://doi.org/10.1128/aem.02320-21.

631 14. Thomashow, L.S., and Weller, D.M. (1988). Role of a phenazine antibiotic from Pseudomonas
632 fluorescens in biological control of Gaeumannomyces graminis var. tritici. J Bacteriol *170*, 3499–
633 3508. https://doi.org/10.1128/jb.170.8.3499-3508.1988.

634 15. Chin-A-Woeng, T.F.C., Bloemberg, G.V., and Lugtenberg, B.J.J. (2003). Phenazines and their role in
635 biocontrol by Pseudomonas bacteria. New Phytologist *157*, 503–523. https://doi.org/10.1046/j.1469-
636 8137.2003.00686.x.

637 16. LeTourneau, M.K., Marshall, M.J., Cliff, J.B., Bonsall, R.F., Dohnalkova, A.C., Mavrodi, D.V.,
638 Devi, S.I., Mavrodi, O.V., Harsh, J.B., Weller, D.M., et al. (2018). Phenazine-1-carboxylic acid and
639 soil moisture influence biofilm development and turnover of rhizobacterial biomass on wheat root
640 surfaces. Environmental Microbiology *20*, 2178–2194. https://doi.org/10.1111/1462-2920.14244.

641 17. Fuqua, W.C., Winans, S.C., and Greenberg, E.P. (1994). Quorum sensing in bacteria: the LuxR-LuxI
642 family of cell density-responsive transcriptional regulators. J Bacteriol *176*, 269–275.
643 https://doi.org/10.1128/jb.176.2.269-275.1994.

644 18. Venturi, V. (2006). Regulation of quorum sensing in Pseudomonas. FEMS Microbiol Rev *30*, 274–
645 291. https://doi.org/10.1111/j.1574-6976.2005.00012.x.

646 19. Miller, M.B., and Bassler, B.L. (2001). Quorum Sensing in Bacteria. Annual Review of
647 Microbiology *55*, 165–199. https://doi.org/10.1146/annurev.micro.55.1.165.

648 20. Waters, C.M., and Bassler, B.L. (2005). QUORUM SENSING: Cell-to-Cell Communication in
649 Bacteria. Annual Review of Cell and Developmental Biology *21*, 319–346.
650 https://doi.org/10.1146/annurev.cellbio.21.012704.131001.

651 21. Parsek, M.R., and Greenberg, E.P. (2005). Sociomicrobiology: the connections between quorum
652 sensing and biofilms. Trends Microbiol *13*, 27–33. https://doi.org/10.1016/j.tim.2004.11.007.

653 22. Papenfort, K., and Bassler, B.L. (2016). Quorum sensing signal–response systems in Gram-negative
654 bacteria. Nat Rev Microbiol *14*, 576–588. https://doi.org/10.1038/nrmicro.2016.89.

655 23. Abisado, R.G., Benomar, S., Klaus, J.R., Dandekar, A.A., and Chandler, J.R. (2018). Bacterial
656 Quorum Sensing and Microbial Community Interactions. mBio *9*, e02331-17.
657 https://doi.org/10.1128/mBio.02331-17.

658 24. Whiteley, M., Diggle, S.P., and Greenberg, E.P. (2017). Bacterial quorum sensing: the progress and
659 promise of an emerging research area. Nature *551*, 313–320. https://doi.org/10.1038/nature24624.

660 25. Mukherjee, S., and Bassler, B.L. (2019). Bacterial quorum sensing in complex and dynamically
661 changing environments. Nat Rev Microbiol *17*, 371–382. https://doi.org/10.1038/s41579-019-0186-5.

662 26. Raynaud, X., and Nunan, N. (2014). Spatial Ecology of Bacteria at the Microscale in Soil. PLOS
663 ONE *9*, e87217. https://doi.org/10.1371/journal.pone.0087217.

664 27. Wang, G., and Or, D. (2010). Aqueous films limit bacterial cell motility and colony expansion on
665 partially saturated rough surfaces. Environmental Microbiology *12*, 1363–1373.
666 https://doi.org/10.1111/j.1462-2920.2010.02180.x.

667 28. Tecon, R., and Or, D. (2017). Biophysical processes supporting the diversity of microbial life in soil.
668 FEMS Microbiol Rev *41*, 599–623. https://doi.org/10.1093/femsre/fux039.

669 29. Mavrodi, D.V., Mavrodi, O.V., Parejko, J.A., Bonsall, R.F., Kwak, Y.-S., Paulitz, T.C., Thomashow,
670 L.S., and Weller, D.M. (2012). Accumulation of the Antibiotic Phenazine-1-Carboxylic Acid in the
671 Rhizosphere of Dryland Cereals. Applied and Environmental Microbiology *78*, 804–812.
672 https://doi.org/10.1128/AEM.06784-11.

673 30. Mavrodi, D.V., Mavrodi, O.V., Elbourne, L.D.H., Tetu, S., Bonsall, R.F., Parejko, J., Yang, M.,
674 Paulsen, I.T., Weller, D.M., and Thomashow, L.S. (2018). Long-Term Irrigation Affects the
675 Dynamics and Activity of the Wheat Rhizosphere Microbiome. Front. Plant Sci. *9*.
676 https://doi.org/10.3389/fpls.2018.00345.

677 31. Schuhegger, R., Ihring, A., Gantner, S., Bahnweg, G., Knappe, C., Vogg, G., Hutzler, P., Schmid, M.,
678 Van Breusegem, F., Eberl, L., et al. (2006). Induction of systemic resistance in tomato by N-acyl-L-
679 homoserine lactone-producing rhizosphere bacteria. Plant Cell Environ *29*, 909–918.
680 https://doi.org/10.1111/j.1365-3040.2005.01471.x.

681 32. DeAngelis, K.M., Firestone, M.K., and Lindow, S.E. (2007). Sensitive Whole-Cell Biosensor
682 Suitable for Detecting a Variety of N-Acyl Homoserine Lactones in Intact Rhizosphere Microbial
683 Communities. Appl Environ Microbiol *73*, 3724–3727. https://doi.org/10.1128/AEM.02187-06.

684 33. DeAngelis, K.M., Lindow, S.E., and Firestone, M.K. (2008). Bacterial quorum sensing and nitrogen
685 cycling in rhizosphere soil. FEMS Microbiol Ecol *66*, 197–207. https://doi.org/10.1111/j.1574-
686 6941.2008.00550.x.

687 34. Redfield, R.J. (2002). Is quorum sensing a side effect of diffusion sensing? Trends in Microbiology
688 *10*, 365–370. https://doi.org/10.1016/S0966-842X(02)02400-9.

689 35. Hense, B.A., Kuttler, C., Müller, J., Rothballer, M., Hartmann, A., and Kreft, J.-U. (2007). Does
690 efficiency sensing unify diffusion and quorum sensing? Nat Rev Microbiol *5*, 230–239.
691 https://doi.org/10.1038/nrmicro1600.

692 36. Platt, T.G., and Fuqua, C. (2010). What's in a name? The semantics of quorum sensing. Trends
693 Microbiol *18*, 383–387. https://doi.org/10.1016/j.tim.2010.05.003.

694 37. West, S.A., Winzer, K., Gardner, A., and Diggle, S.P. (2012). Quorum sensing and the confusion
695 about diffusion. Trends in Microbiology *20*, 586–594. https://doi.org/10.1016/j.tim.2012.09.004.

696 38. Boedicker, J.Q., Vincent, M.E., and Ismagilov, R.F. (2009). Microfluidic Confinement of Single
697 Cells of Bacteria in Small Volumes Initiates High-Density Behavior of Quorum Sensing and Growth
698 and Reveals Its Variability. Angewandte Chemie International Edition *48*, 5908–5911.
699 https://doi.org/10.1002/anie.200901550.

700 39. Darch, S.E., Simoska, O., Fitzpatrick, M., Barraza, J.P., Stevenson, K.J., Bonnecaze, R.T., Shear,
701 J.B., and Whiteley, M. (2018). Spatial determinants of quorum signaling in a Pseudomonas
702 aeruginosa infection model. Proceedings of the National Academy of Sciences *115*, 4779–4784.
703 https://doi.org/10.1073/pnas.1719317115.

704 40. Stewart, P.S. (2003). Diffusion in Biofilms. Journal of Bacteriology *185*, 1485–1491.
705 https://doi.org/10.1128/jb.185.5.1485-1491.2003.

706 41. Parsek, M.R., and Greenberg, E.P. (2005). Sociomicrobiology: the connections between quorum
707 sensing and biofilms. Trends Microbiol *13*, 27–33. https://doi.org/10.1016/j.tim.2004.11.007.

708 42. Kim, M.K., Ingremeau, F., Zhao, A., Bassler, B.L., and Stone, H.A. (2016). Local and global
709 consequences of flow on bacterial quorum sensing. Nat Microbiol *1*, 15005.
710 https://doi.org/10.1038/nmicrobiol.2015.5.

711 43. Hense, B.A., Müller, J., Kuttler, C., and Hartmann, A. (2012). Spatial Heterogeneity of Autoinducer
712 Regulation Systems. Sensors *12*, 4156–4171. https://doi.org/10.3390/s120404156.

713 44. Thomashow, L.S., and Weller, D.M. (1988). Role of a phenazine antibiotic from Pseudomonas
714 fluorescens in biological control of Gaeumannomyces graminis var. tritici. J Bacteriol *170*, 3499–
715 3508. https://doi.org/10.1128/jb.170.8.3499-3508.1988.

716 45. Mavrodi, D.V., Ksenzenko, V.N., Bonsall, R.F., Cook, R.J., Boronin, A.M., and Thomashow, L.S.
717 (1998). A Seven-Gene Locus for Synthesis of Phenazine-1-Carboxylic Acid by Pseudomonas
718 fluorescens 2-79. J Bacteriol *180*, 2541–2548.

719 46. Khan, S.R., Mavrodi, D.V., Jog, G.J., Suga, H., Thomashow, L.S., and Farrand, S.K. (2005).
720 Activation of the phz Operon of Pseudomonas fluorescens 2-79 Requires the LuxR Homolog PhzR,

N-(3-OH-Hexanoyl)-l-Homoserine Lactone Produced by the LuxI Homolog PhzI, and a cis-Acting phz Box. J Bacteriol *187*, 6517–6527. https://doi.org/10.1128/JB.187.18.6517-6527.2005.

47. Khan, S.R., Herman, J., Krank, J., Serkova, N.J., Churchill, M.E.A., Suga, H., and Farrand, S.K. (2007). N-(3-Hydroxyhexanoyl)-l-Homoserine Lactone Is the Biologically Relevant Quormone That Regulates the phz Operon of Pseudomonas chlororaphis Strain 30-84. Applied and Environmental Microbiology *73*, 7443–7455. https://doi.org/10.1128/AEM.01354-07.

48. Zhang, O., Alcalde, R.E., Zhou, H., Yin, S., Newman, D.K., and Yang, C. (2024). Investigating 3D microbial community dynamics of the rhizosphere using quantitative phase and fluorescence microscopy. Proceedings of the National Academy of Sciences *121*, e2403122121. https://doi.org/10.1073/pnas.2403122121.

49. Holford, I.C.R. (1997). Soil phosphorus: its measurement, and its uptake by plants. Soil Res. *35*, 227–240. https://doi.org/10.1071/s96047.

50. Hinsinger, P. (2001). Bioavailability of soil inorganic P in the rhizosphere as affected by root-induced chemical changes: a review. Plant and Soil *237*, 173–195. https://doi.org/10.1023/A:1013351617532.

51. Ducousso-Détrez, A., Fontaine, J., Lounès-Hadj Sahraoui, A., and Hijri, M. (2022). Diversity of Phosphate Chemical Forms in Soils and Their Contributions on Soil Microbial Community Structure Changes. Microorganisms *10*, 609. https://doi.org/10.3390/microorganisms10030609.

52. Whooley, M.A., and McLoughlin, A.J. (1982). The regulation of pyocyanin production in Pseudomonas aeruginosa. European J. Appl. Microbiol. Biotechnol. *15*, 161–166. https://doi.org/10.1007/BF00511241.

53. Jensen, V., Löns, D., Zaoui, C., Bredenbruch, F., Meissner, A., Dieterich, G., Münch, R., and Häussler, S. (2006). RhlR Expression in Pseudomonas aeruginosa Is Modulated by the Pseudomonas Quinolone Signal via PhoB-Dependent and -Independent Pathways. JB *188*, 8601–8606. https://doi.org/10.1128/JB.01378-06.

54. Oglesby, A.G., Farrow, J.M., Lee, J.-H., Tomaras, A.P., Greenberg, E.P., Pesci, E.C., and Vasil, M.L. (2008). The influence of iron on Pseudomonas aeruginosa physiology: a regulatory link between iron and quorum sensing. J Biol Chem *283*, 15558–15567. https://doi.org/10.1074/jbc.m707840200.

55. Lee, J., Wu, J., Deng, Y., Wang, J., Wang, C., Wang, J., Chang, C., Dong, Y., Williams, P., and Zhang, L.-H. (2013). A cell-cell communication signal integrates quorum sensing and stress response. Nat Chem Biol *9*, 339–343. https://doi.org/10.1038/nchembio.1225.

56. Nguyen, A.T., Jones, J.W., Ruge, M.A., Kane, M.A., and Oglesby-Sherrouse, A.G. (2015). Iron Depletion Enhances Production of Antimicrobials by Pseudomonas aeruginosa. J Bacteriol *197*, 2265–2275. https://doi.org/10.1128/JB.00072-15.

57. Welsh, M.A., and Blackwell, H.E. (2016). Chemical Genetics Reveals Environment-Specific Roles for Quorum Sensing Circuits in *Pseudomonas aeruginosa*. Cell Chemical Biology *23*, 361–369. https://doi.org/10.1016/j.chembiol.2016.01.006.

58. Meng, X., Ahator, S.D., and Zhang, L.-H. (2020). Molecular Mechanisms of Phosphate Stress Activation of Pseudomonas aeruginosa Quorum Sensing Systems. mSphere *5*, 10.1128/msphere.00119-20. https://doi.org/10.1128/msphere.00119-20.

59. Monds, R.D., Newell, P.D., Schwartzman, J.A., and O'Toole, G.A. (2006). Conservation of the Pho regulon in Pseudomonas fluorescens Pf0-1. Appl Environ Microbiol *72*, 1910–1924. https://doi.org/10.1128/AEM.72.3.1910-1924.2006.

60. Hsieh, Y.-J., and Wanner, B.L. (2010). Global Regulation by the Seven-component Pi Signaling System. Curr Opin Microbiol *13*, 198–203. https://doi.org/10.1016/j.mib.2010.01.014.

61. Santos-Beneit, F. (2015). The Pho regulon: a huge regulatory network in bacteria. Front. Microbiol. *6*. https://doi.org/10.3389/fmicb.2015.00402.

62. Goldberg, S., and Sposito, G. (1984). A Chemical Model of Phosphate Adsorption by Soils: I. Reference Oxide Minerals. Soil Science Soc of Amer J *48*, 772–778. https://doi.org/10.2136/sssaj1984.03615995004800040015x.

63. Dzombak, D.A., and Morel, F. (1990). Surface complexation modeling: hydrous ferric oxide (Wiley).

64. Boyd, V., Yoon, H., Zhang, C., Oostrom, M., Hess, N., Fouke, B., Valocchi, A.J., and Werth, C.J. (2014). Influence of Mg2+ on CaCO3 precipitation during subsurface reactive transport in a homogeneous silicon-etched pore network. Geochimica et Cosmochimica Acta *135*, 321–335. https://doi.org/10.1016/j.gca.2014.03.018.

65. van Delden, C., Comte, R., and Bally, A.M. (2001). Stringent Response Activates Quorum Sensing and Modulates Cell Density-Dependent Gene Expression inPseudomonas aeruginosa. Journal of Bacteriology *183*, 5376–5384. https://doi.org/10.1128/jb.183.18.5376-5384.2001.

66. Diggle, S.P., Winzer, K., Chhabra, S.R., Worrall, K.E., Cámara, M., and Williams, P. (2003). The Pseudomonas aeruginosa quinolone signal molecule overcomes the cell density-dependency of the quorum sensing hierarchy, regulates rhl-dependent genes at the onset of stationary phase and can be produced in the absence of LasR. Molecular Microbiology *50*, 29–43. https://doi.org/10.1046/j.1365-2958.2003.03672.x.

67. Dubern, J.-F., Halliday, N., Cámara, M., Winzer, K., Barrett, D.A., Hardie, K.R., and Williams, P. (2023). Growth rate and nutrient limitation as key drivers of extracellular quorum sensing signal molecule accumulation in Pseudomonas aeruginosa. Microbiology *169*, 001316. https://doi.org/10.1099/mic.0.001316.

68. W. G. Sunda, N. M. Price, and F. M. M. Morel (2005). Algal culturing techniques R. A. Andersen, ed. (Elsevier/Academic Press).

69. Choi, K.-H., and Schweizer, H.P. (2006). mini-Tn 7 insertion in bacteria with single att Tn 7 sites: example Pseudomonas aeruginosa. Nat Protoc *1*, 153–161. https://doi.org/10.1038/nprot.2006.24.